JSEE Vol. 24, No. 3&4, 2022 DOI: 10.48303/jsee.2023.1986674.1043

Research Paper

A Novel Numerical Iterative Procedure for Ground Motion Simulation

Roohollah M. Pirooz

M.Sc. Graduate of Structural Engineering, Civil Engineering Department, School of Engineering, University of Kharazmi, Tehran, Iran, rmpirooz@gmail.com

Received: 03/01/2023
Revised: 28/03/2023
Accepted: 17/05/2023

ABSTRACT

Time history analysis of structures requires some carefully selected earthquake records to be employed as the input for dynamic analysis. Despite the increase in number of recorded earthquake ground motions, the need for generation of artificial accelerograms is highly demanded in some areas for some reason. As a result, many efforts have been made to develop mathematical methods for simulating ground motions by various researchers. Since most of the methods for generation of spectrum compatible signals use relatively complex mathematical approaches, it requires engineers to make more effort and spend time to deal with these complicated methods. In order to meet engineers' demand for generation of the above-mentioned signals while maintaining an applicable tool that is easy to utilize, a simple, numerically iterative novel procedure has been proposed based on the linear combination of intrinsic mode functions (IMF) of recorded seismic signals evaluated by empirical mode decomposition (EMD). The proposed method requires only basics of structural dynamics and definitely all engineers are familiar with them and simply can apply the method, while it leads to results as accurate and efficient as benchmark methods such as random vibration theory and time-frequency analysis techniques. The results of this study prove the applicability of the developed approach.

Keywords:
Ground motion simulation;
Empirical mode decomposition;
Over-determined system of equations

1. Introduction

Seismic codes apply restrict provisions on how to select and scale earthquake records for time history analysis. For example, Iran seismic code (Standard 2800) states that the selected records should be seismically compatible with construction site from magnitude, distance to source, soil type and duration point of views. Also, selected records should be scaled with respect to standard design spectrum (Iranian Code of Practice for Seismic Resistant Design of Buildings, 2017). Such provisions make the availability of real accelerograms to be a challenging issue in some cases. Even if actual seismic signals are available, they might not be compatible with design spectrum defined by codes.

Above-mentioned issues, led researchers to employ a wide variety of mathematical approaches and techniques such as random vibration, time-frequency analysis, probability theory and statistics to generate artificial records, which satisfy required provisions. Synthetizing artificial ground motion signals are widely discussed in the literature.

In this regard, Nonstationary Kanai-Tajimi model (Rofooei et al., 2001; Bani-Hani et al., 2017), modulating harmonic cosine signals and sinusoidal waves (Gomes et al., 2006; Li et al., 2017), evolutionary power spectrum procedure (Zhang et al., 2007; Cacciola & Zentner, 2012) and auto-regressive moving-average (Spanos et al., 2009) were employed to generate artificial accelerograms. In another try, time domain procedures

have been utilized to generate spatially correlated nonstationary ground motions (Liu et al., 2009).

Also, applications of evolutionary cross-spectral matrix and random perturbations (Shields, 2015) and energy distribution in time and frequency content (Carli & Carino, 2016) to synthesize seismic signals have been shown.

Spectrum compatible artificial records have been synthesized employing random standard Gaussian numbers and a piecewise windowing function (Tehrani & Harvey, 2019) and also by introducing non-stationary to stationary random time series using an envelope function and changing frequency content (Parajuli & Shrestha, 2018). By solving an over-determined system, a non-iterative procedure was developed to generate non-stationary stochastic processes compatible with uniform hazard spectrum (Giaralis & Spanos, 2012). The application of modulating white noise sequence to generate synthetic time-histories was also discussed (Vetter et al., 2016; Tsioulou, et al. 2018). In another work, the effect of distribution of peak ground displacement has been investigated in generation of artificial seismograms by Wang et al. (2019).

Also, methods based on time-frequency analysis techniques have extent application in synthesizing artificial accelerograms with different approaches (Suarez & Montejo, 2005; Giaralis & Spanos, 2009; Shama, 2012; Cecini & Palmeri, 2015; Mukhopadhyay et al., 2019). For example, modified L-P wavelet to simulate aftershock events (Das & Gupta, 2008), S-transform to adjust frequency content of earthquake ground motion (Fan et al., 2010), Hilbert-Huang transform for generation of spectrum compatible accelerograms (Vrochidou et al., 2014, 2018), Utilizing wavelet analysis to generate nonstationary near-fault time histories (Amiri et al., 2014) and applying modified Littlewood-Paley wavelet for simulation of spatially correlated accelerograms (Sarkar et al., 2016) can be mentioned. Adding wavelets and adjustment of real earthquake records by continuous wavelet transform and using Fourier transform approach were discussed and compared by Gascot and Montejo (2016). Furthermore, a time-frequency modulation function has been proposed for generation of fully nonstationary earthquake records (Wang et al., 2021).

An iterative approach by applying harmonic wavelets was used to synthesize tri-component ground motions (Trovato et al., 2017). A stochastic method of simulation and modification has been developed to generate energy and spectrum compatible synthetic ground motions using wavelet packets (Huang & Wang, 2017). In this regard, using wavelet transform and Baker's method, it is tried to preserve strong velocity pulse of near fault records due to forward directivity effects during spectral matching (Gholizad & Pursadrollah, 2017).

Also, the applicability of neural network method to synthesize artificial records has been demonstrated by several researchers. This method is usually used in conjunction with one or more of wavelet transform, principal component analysis, optimization methods and etc. (Rajasekaran et al., 2006; Amiri et al., 2009, 2012; Rajabi & Ghodrati Amiri, 2020). By setting the upper bound of earthquake input energy per unit mass as a constraint, synthetic accelerograms were generated as critical excitation for multi-degree of freedom systems (Bazrafshan & Khaji, 2020).

Finally, it is possible to mention other techniques such as maximum entropy principle (Batou & Soize, 2014), Latin hypercube sampling (Mitropoulou et al., 2015) and probabilistic approaches (Brewick et al., 2018) for generation of spectrum compatible ground motions.

Extensive research and the use of various techniques for generation of artificial accelerograms show the significant importance of this issue. Each of the methods developed by various researchers offers their specific advantages, meanwhile they might be complicated to implement. In order to apply these methods, one needs to be familiar with theories or techniques such as random vibrations, time-frequency analysis, statistics and probability, or even neural networks and genetic algorithms. The author's experience shows that engineers are generally unfamiliar with such methods and have difficulty utilizing them in real projects. Although some software has been developed to synthesize seismic signals, deep knowledge of basics and familiarity with implementation details are required to get use of it in an efficient way.

Therefore, it can be expected that a simple method, which leads to results as good as common developed techniques, will be welcomed by the engineering community. In this study, a novel method for the generation of spectrum compatible accelerograms is presented that familiarity with basics of structural dynamics (linear dynamic analysis of single-degree of free systems and response spectrum) suffices for efficient application of it. This method can readily be programmed by numerical packages such as MATLAB or Python to be employed. Results of this work confirm the accuracy of the proposed method. The introduced method can be employed effectively for modifying seed records such that they get compatible with target spectrum.

2. Theoretical Background

The developed procedure can be summarized in following steps:

1. Specify target spectrum and the desired period range for spectral matching.
2. Select as many as required actual records for modification.
3. Use empirical mode decomposition method to decompose selected seismic signals to their intrinsic mode functions (IMF).
4. Apply appropriate scale factors to IMFs, such that the summation of them leads to a signal, compatible with the target spectrum.

Each step would be explained in the following sections in more details.

2.1. Target Spectrum

Constructing target spectrum depends on the provisions of seismic code which must be applied. In this study, standard design spectrum defined by Iran seismic code with 10% probability of exceedance in 50 years with return period of 475 years was used for period interval of zero to 3.0 sec.

The spectrum was constructed for a site with very high seismic activity (A=0.35, ratio of base design acceleration to gravitational acceleration) and soil type II (375 < V_{S30} < 750 m/sec, average shear wave velocity of top 30 m of the site). Standard design spectrum (Sa_t, as target spectrum) can be evaluated by Equation (1). In this equation, B is building reflection factor defined in Equation (2):

$$Sa_t = ANB \tag{1}$$

$$B = B_1 N \tag{2}$$

where B_1 is the spectrum shape factor (Equation 2.1), and N is spectrum correction factor, which can be evaluated for very high seismic activity and soil type II by Equation (2.2).

$$\begin{aligned} B_1 &= S_0 + (S - S_0 + 1)\left(\frac{T}{T_0}\right) && 0.0 < T < T_0 \\ B_1 &= S + 1 && T_0 < T < T_s \\ B_1 &= (S+1)\left(\frac{T_s}{T}\right) && T > T_s \end{aligned} \tag{2.1}$$

$$\begin{aligned} N &= 1 && T < T_s \\ N &= \frac{0.7}{4 - T_s}(T - T_s) + 1 && T_s < T < 4 \text{ sec} \\ N &= 1.7 && T > 4 \text{ sec} \end{aligned} \tag{2.2}$$

In Equations (2.1) and (2.2), T, T_0, T^s, S_0 and S are period in second, 0.1 sec, 0.5 sec, 1 and 1.5 respectively as defined by Iran seismic code for aforementioned site conditions. Finally, the target spectrum used in this study for period range of zero to 3.0 sec is shown in Figure (1).

2.2. Selected Records

All developed methods for simulation of seismic signals requires a seed record. This seed record can be a string of random numbers or an actual earthquake record. Then, by modifying the seed record, its frequency content would be adjusted, such that its response spectrum becomes compatible with the prescribed target. To this end, actual earthquake records have been used as seed.

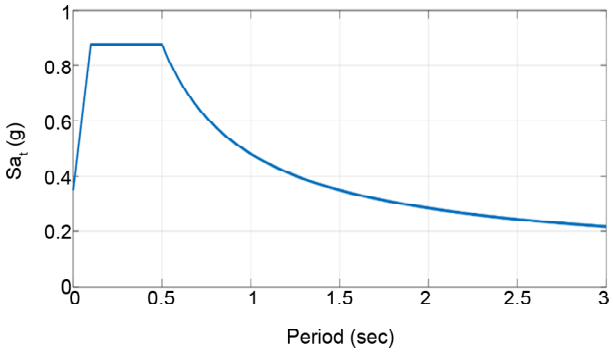

Figure 1. Target spectrum for period range of zero to 3.0 sec.

Using a string of random numbers require some mathematical manipulations such that they can resemble an earthquake ground motion as much as possible, which might be challenging for some engineers. It is also worth mentioning that although there is no single actual accelerogram fully compatible with design spectra defined by seismic codes, but nowadays there are large databases of these records freely available. As a result, using actual earthquake records seem more reasonable.

In this study, 21 horizontal components of actual earthquakes have been selected to be used as seed records. The developed procedure in this study will be applied to these records to synthesize new seismic signals with desired frequency content. This will validate the applicability of the proposed method for synthesizing seismic signals.

Table (1) shows the main characteristics of selected records. Hereafter, when it is required to mention an earthquake, its assigned ID as shown in Table (1) will be referred. The selected records have the magnitude range of 6.0 to 7.62. V_{S30} is between 375 and 750 m/sec, and the closest distance to the causative fault is less than 10 km.

It should be noted that seismic codes apply some regulations for selection of earthquake records to be input for dynamic analysis. For example, the soil type for the selected records must be the same, and the effects of magnitude and distance from the causative fault must be taken into account. As a result, near-fault earthquake ground motions, which are recorded on soil type II were selected to be used in this study. Although after modification of seed records to make them compatible with target spectrum, their frequency content may alter significantly, but it is tried to satisfy the Iran seismic code provisions for earthquake records selection.

2.3. Empirical Mode Decomposition (EMD)

EMD is a technique which can be applied to decompose nonstationary signals (such as earthquake records) into their intrinsic mode functions (IMFs) (Vrochidou et al., 2014). It would result in few numbers of IMFs and one residual (r). The first IMF, contains highest frequency waves and the later, the lowest ones. After decomposition, the original accelerogram $a(t)$ can be reconstructed

Table 1. Selected Records.

ID	Earthquake Name	Station Name	Magnitude	R[1]	V_{S30}[2]	PGA[3]
EQ01	Helena, Montana-01	Carroll College	6	2.86	593.35	0.16
EQ02	Helena, Montana-02	Helena Fed Bldg	6	2.92	551.82	0.05
EQ03	Morgan Hill	Coyote Lake Dam Southwest Abutment	6.19	0.53	561.43	0.71
EQ04	Nahanni, Canada	Site 3	6.76	5.32	605.04	0.17
EQ05	Kalamata, Greece-01	Kalamata (bsmt)	6.2	6.45	382.21	0.24
EQ06	Loma Prieta	Gilroy - Gavilan Coll.	6.93	9.96	729.65	0.33
EQ07	Northridge-01	Jensen Filter Plant Generator Building	6.69	5.43	525.79	0.99
EQ08	Northridge-01	Sylmar - Olive View Med FF	6.69	5.3	440.54	0.84
EQ09	Chi-Chi, Taiwan	CHY028	7.62	3.12	542.61	0.76
EQ10	Chi-Chi, Taiwan-03	TCU078	6.2	7.62	443.04	0.27
EQ11	Parkfield-02, CA	PARKFIELD-DONNA LEE	6	4.93	656.75	0.37
EQ12	Parkfield-02, CA	PARKFIELD-STOCKDALE MTN	6	4.83	393.56	0.23
EQ13	Parkfield-02, CA	Parkfield - Cholame 2E	6	4.08	522.74	0.51
EQ14	Parkfield-02, CA	Parkfield - Cholame 3E	6	5.55	397.36	0.52
EQ15	Parkfield-02, CA	Parkfield - Fault Zone 11	6	4	541.73	0.60
EQ16	Parkfield-02, CA	Parkfield - Vineyard Cany 2W	6	3.52	438.74	0.38
EQ17	Niigata, Japan	NIG028	6.63	9.79	430.71	0.85
EQ18	Umbria Marche, Italy	Nocera Umbra	6	8.92	428	0.47
EQ19	Christchurch, New Zealand	Heathcote Valley Primary School	6.2	3.36	422	1.29
EQ20	Christchurch, New Zealand	LPCC	6.2	6.12	649.67	0.91
EQ21	Bam	Bam	6.6	1.7	484.7	0.81

R: Closest distance from recording station to earthquake causing fault (kilometer)

V_{s30}: Average shear wave velocity of top 30 m of the site (m/sec)

PGA: Peak ground acceleration (g)

as shown in Equation (3):

$$a(t)=\sum_{j=1}^{m-1} IMF_j(t)+r(t) \tag{3}$$

In this work, the number of IMFs is considered to be m - 1. As a result, from Equation (3) it can be inferred that the summation of m - 1 number of IMFs plus one residual, reconstruct the original signal $a(t)$. The total number of IMFs and one residual are m signals, which hereafter, they would be called base signals $(S_b(t))$. Consequently, Equation (3) can be rewritten as follows:

$$a(t)=\sum_{j=1}^{m} S_b^j(t) \tag{4}$$

The following steps demonstrate how to use EMD to extract IMFs of a signal:

1. Construct the upper and lower envelopes of original signal $a(t)$ ($U(t)$ and $L(t)$ respectively). This can simply be done by straight lines that connect the local extrema as shown in Figure (2) for EQ02. Calculate $m(t)$, that is the mean of $U(t)$ and $L(t)$ using Equation (5):

$$m(t)=\frac{U(t)+L(t)}{2} \tag{5}$$

2. Subtract $m(t)$ from $a(t)$ to evaluate $f_{11}(t)$.
3. Consider $f_{11}(t)$ as a new signal and repeat steps one and two N times to evaluate $f_1N(t)$. If number of extrema and zero crossings are equal or differ at most by one value, and the mean of upper and lower envelopes of $f_1N(t)$ for whole duration of signal equals to zero, $f_1N(t)$ is considered as $MF_1(t)$.
4. Subtract $IMF_1(t)$ from the original signal to evaluate f21(t). Repeat step three to evaluate $IMF_2(t)$.
5. Do the same to evaluate all IMFs and reach residual $r(t)$. $r(t)$ should be a monotonic function or its peak value be less than a specified value. At this point, all of possible IMFs have been determined and iterations must be stopped.

Figure (3) shows ground acceleration time history of *EQ*01 and its first, fifth and last base signal. It is worth noting that $S_b^{14}(t)$. (last base signal) is a decreasing monotonic function as it was stated in step 5.

2.4. Scaling of Base Signals

As mentioned earlier, the summation of base signals (Equation 4) reconstructs the original signal. As a result, any linear combination of base signals would result in a new signal $A(t)$, as shown in Equation (6):

$$A(t)=\sum_{j=1}^{m}\alpha_j S_b^j(t) \qquad \alpha_j : \textit{scale factor} \tag{6}$$

1. It is aimed to find $\alpha_j s$, such that the resulting response spectrum of $A(t)$ be compatible with target spectrum. To do so, the following steps should be followed:
2. Calculate acceleration response time history $(R_{ij}(t))$ of linear single degree of freedom system (SDOF) with period T_i subjected to $S_b^j(t)$. $R_{ij}(t)$ denotes the response of SDOF system with period T_i subjected to $S_b^j(t)$.

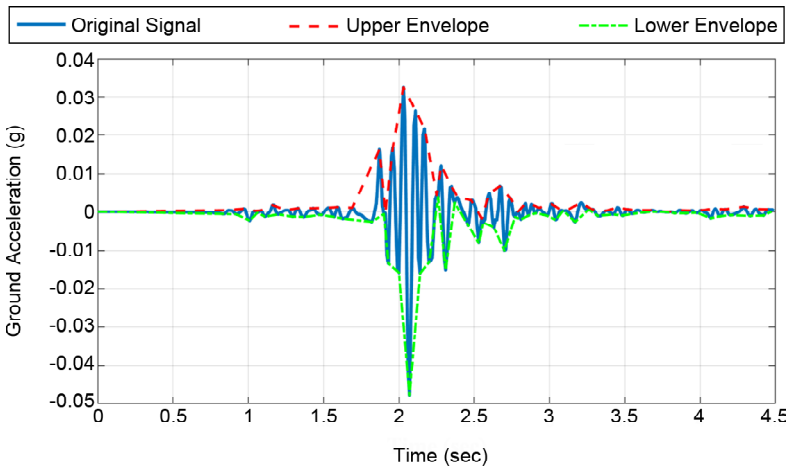

Figure 2. Ground acceleration of EQ02 and its upper and lower envelopes.

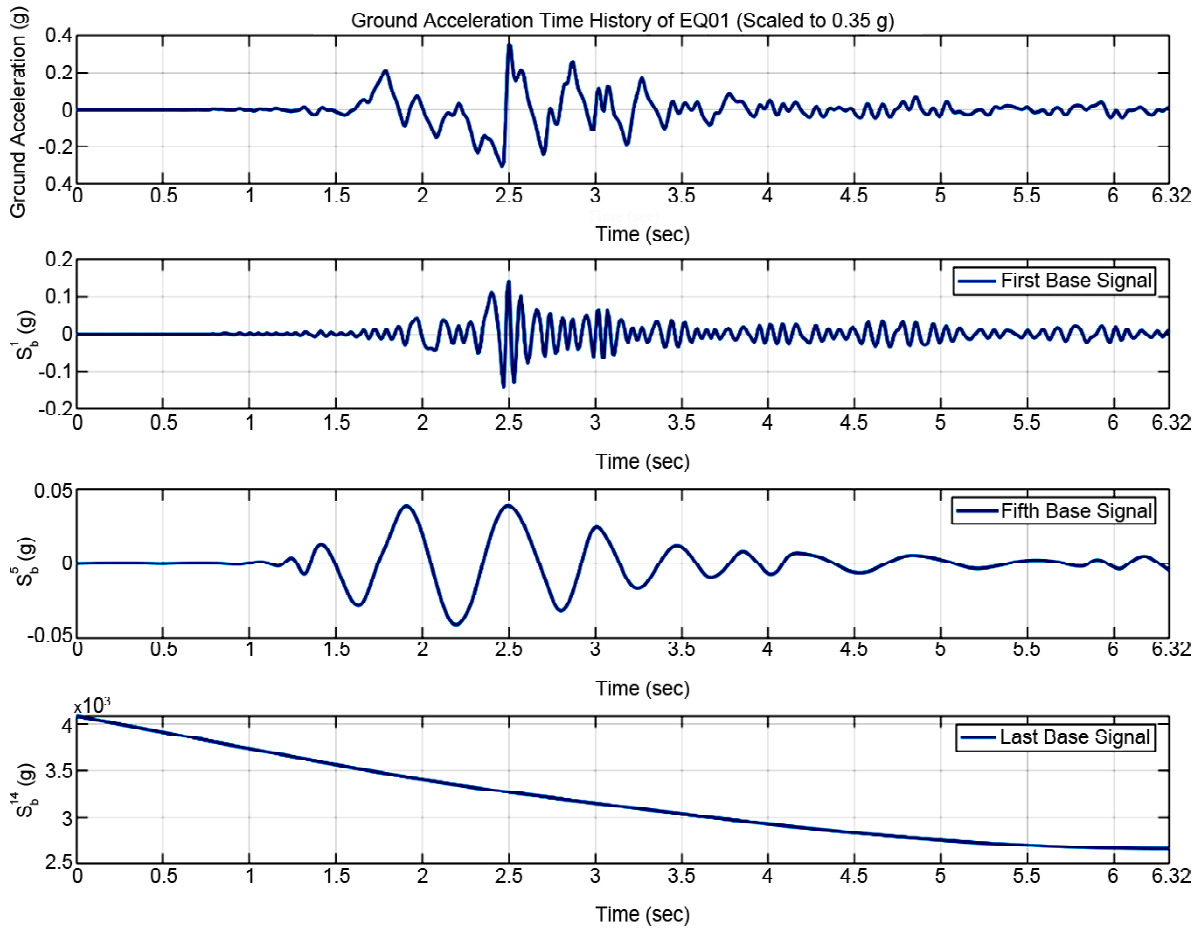

Figure 3. Acceleration time history of EQ01 and its corresponding base signals.

Construct the system of equations as in Equation (7.1):

$$\begin{aligned} &max\left|R_{11}(t)\,\alpha_1+\ldots+R_{1m}(t)\,\alpha_m\right|=Sa_t(T_1)\\ &max\left|R_{21}(t)\,\alpha_1+\ldots+R_{2m}(t)\,\alpha_m\right|=Sa_t(T_2)\\ &\qquad\vdots\\ &max\left|R_{n1}(t)\,\alpha_1+\ldots+R_{nm}(t)\,\alpha_m\right|=Sa_t(T_n) \end{aligned} \tag{7.1}$$

Or in matrix form, it can be demonstrated as Equation (7.2):

$$max\begin{bmatrix} R_{11}(t) & \cdots & R_{1m}(t)\\ R_{21}(t) & \cdots & R_{2m}(t)\\ \vdots & \vdots & \vdots\\ R_{n1}(t) & \cdots & R_{nm} \end{bmatrix}\begin{bmatrix}\alpha_1\\ \alpha_2\\ \vdots\\ \alpha_m\end{bmatrix}=\begin{bmatrix}Sa_t(T_1)\\ Sa_t(T_2)\\ \vdots\\ Sa_t(T_n)\end{bmatrix} \tag{7.2}$$

The symbols max and |…| denote the maximum and absolute value operators. The left side of Equation (7.2) is response spectrum (Sa) of seismic signal $A(t)$ and the right side is target spectrum Sa_t. In this equation, the ideal state is obtained if both sides are exactly equal. That is, the response spectrum of $A(t)$ becomes fully compatible with the target spectrum.

3. Set $\alpha_2=\alpha_3=\ \ldots=\ \alpha_m=1$ and evaluate α_1 such that the desired criterion gets as minimum as possible (criteria to be minimized and procedure to evaluate each α_j will be discussed in sections 2.5 and 2.6, respectively).
4. Given the α_1 from previous step, evaluate α_2 while set rest of $\alpha_j s\ =1$.
5. Repeat step four, to determine each α_j.
6. Given α_2, α_3, …, α_m from previous steps, recalculate α_1.
7. Do the same for other $\alpha_j s$ until the desired criterion be reached or cannot be decreased anymore.

In most cases, the number of base signals for any decomposed accelerograms is less than the number of T_{is} for the period interval in which the spectral matching should be done. Consequently, Equation (7) is an over-determined system of equations, that is,

the number of equations (n) is greater than the number of unknowns (m). The coefficients of each equation (R_{ijs}) are response of a SDOF system with different periods and this makes the equations to be linearly independent. As a result, there is no exact solution to satisfy the system of equations and just an approximate solution can be achieved with some degree of error.

On the other hand, due to the presence of maximum and absolute value operators in each equation, the conventional algebraic approaches such as least square method cannot be employed to solve the system of equations. In addition, the R_{ijs} that construct the coefficient matrix are each a vector, not a scalar, and this adds to the complexity of the problem. Thus, the iterative procedure described above, should be employed.

Iterations will be continued until the error rate reaches to a prescribed value, or it cannot be decreased anymore. Also, it is possible to set a limit on how much iteration is done. In this work, evaluation of each α_i is defined as a sub iteration and a complete cycle as an iteration.

2.5. Criteria to be Minimized

2.5.1 Minimum Mean Error (MME)

The error (E_i) at each T_i and corresponding mean error (E_m) can be calculated as follows:

$$E_i(\%) = \frac{|Sa_t(T_i) - Sa(T_i)|}{Sa_t(T_i)} \times 100 \tag{8}$$

$$E_m(\%) = \frac{\sum_1^n E_i}{n} \tag{9}$$

In MME method, scale factors should be determined such that Em be minimized. It is clear that as Em gets closer to zero, the shape of S_a and its ordinates would be more compatible with Sa_t.

2.5.2. Minimum Enclosed Area (MEA)

Target spectrum Sa_t can be enclosed by two scaled response spectra of modifying seed record. To do this, calculate β_{max} and β_{min} by Equations (10.1) and (10.2), respectively and multiply them with Sa after each sub iteration to determine Sa_U (upper envelop) and Sa_L (lower envelop) using Equations (11.1) and (11.2):

$$\beta_{max} = \max\left(\frac{Sa_t}{Sa}\right) \tag{10.1}$$

$$\beta_{min} = \min\left(\frac{Sa_t}{Sa}\right) \tag{10.2}$$

$$Sa_U = \beta_{max} Sa \tag{11.1}$$

$$Sa_L = \beta_{min} Sa \tag{11.2}$$

Sa_U and Sa_L touch target spectrum just in one point and for the rest of points, they are above and below the Sa_t respectively. In MEA method, α_{js} would be evaluated such that the area between Sa_U and Sa_L becomes the minimum possible value. It is expected as this area decreases, the spectral shape of Sa gets closer to Sat.

As an example, target spectrum Sa_t and corresponding Sa, Sa_U and Sa_L are shown in Figure (4) for modified EQ05 on the period interval of 0.02 to 1.0.

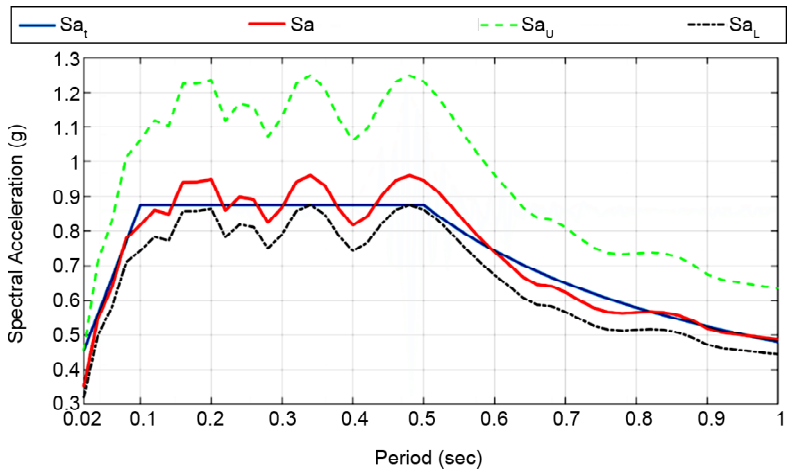

Figure 4. Sa_U and Sa_L for modified EQ05.

Finally, the enclosed area (A_e) between Sa_U and Sa_L on period interval of [T_i T_f] can be determined by Equation (12). It is simply possible to evaluate A_e using numerical integration methods such as trapezoidal.

$$A_e = \int_{T_i}^{T_f} (Sa_U - Sa_L) dT \tag{12}$$

2.6. Calculation method of α_{js}

Consider the first iteration, where it is supposed to evaluate α_1. As stated earlier, set all other α_{js} equal to 1 for $j > 1$. Define an interval of [-x x] with increments of dx for α_1, where x is a real number. For example, in this study, the interval of [-2 2] with increments of 0.01 was considered. Set α_1 equal to each value on the predefined interval and evaluate the left side of Equation (6). In MME method, select that value for α_1 that leads to the lowest value for E_m. On the other hand, in MEA method, find α_1 such that it minimizes A_e. Follow the same procedure for the rest of α_{js}.

Note that, if derived α_j was equal to upper or lower limit of specified interval, this means that, the best solution for α_1 is outside the predefined interval. Therefore, for the next iteration, modify the interval to P% and Q% of that limit, where $P < 100$% and $Q > 100$%. In this work, P and Q were set on 90% and 110%. If the desired criterion would not decrease anymore and none of α_{js} is equal to upper or lower limit of prescribed intervals, extend all intervals by, for example 10% from both sides. This may help iterations find new solutions. If after extending intervals, no new solution was found, iterations must be stopped since the desired criterion has reached its lowest possible value.

Also, it should be mentioned that in MEA method, the response spectrum of signal $A(t)$ would be compressed between Sa_U and Sa_L, and its shape gets as close as possible to the target spectrum. But it may be completely somewhere above or below Sa_t. Thus, after finishing iterations, it is required to apply an overall scale factor to $A(t)$. To do so, using Equations (13.1), (13.2) and (13.3) calculate θ_{max}, θ_{min} and construct the interval θ:

$$\theta_{max} = \max\left(\frac{Sa_t}{Sa}\right) \tag{13.1}$$

$$\theta_{min} = \min\left(\frac{Sa_t}{Sa}\right) \tag{13.2}$$

$$\theta = [\theta_{min} \quad \theta_{max}] \text{ with increment of } d$$

$$\theta = \frac{\theta_{max} - \theta_{min}}{N} \tag{13.3}$$

In this study, N has been chosen as 999 that makes the interval θ contains 1000 values. Multiply Sa with all values in interval θ and determine which one leads to the lowest E_m.

3. Period Intervals for Spectral Matching

According to Iran seismic code, the selected earthquake records for dynamic analysis of the structure under study are required to be scaled such that their response spectrum not to be less than standard design spectrum on period interval of $0.2T_1$ to $1.5T_1$, where T_1 is the fundamental vibrational mode period of the structure.

Since the seismic energy of earthquake record from periods outside the interval of $0.2T_1$ to $1.5T_1$ has little to no effects on overall dynamic response of structure, it seems to be reasonable to perform spectral matching on a period interval selected on the basis of modal characteristics of structures to be analyzed. This will significantly reduce the computational effort required for spectral matching. For example, for a structure with a fundamental period of 2.0 sec, modes with periods shorter than 0.4 sec have almost no contribution to the dynamic response of the structure. To this end, three period intervals have been selected such that it can reasonably represent the period range of most conventional buildings.

Based on the issues mentioned in previous paragraph, three period intervals (from T_i to T_f, initial and final periods of the interval for spectral matching respectively) were selected to investigate the performance of proposed method on different periods. Also, to provide a basis for making comparison between records, all of them have been scaled to 0.35 g before triggering iterations. The value of 0.35 g was selected due to the fact that $Sa_t(T = 0)$ is equal to 0.35 g. Selected period intervals are shown in Table (2).

Table 2. Period intervals in seconds for spectral matching.

T_i (Initial Period)	T_f (Final Period)	dT (Increment)	No. of Data Points
0.02	1.00	0.02	50
0.10	1.50	0.02	71
0.40	3.00	0.02	131

4. Results and Discussions

The procedure described in section 2 was applied to modify seed records and new accelerograms have been generated. The results show that the proposed method is well able to synthesize seismic signals. As it is expected, the level of spectral matching differs for different seed records. The results of both MME and MEA methods will be examined in next sections.

5. Results of MME Method

Figure (5) depicts as recorded and modified ground motion of EQ21 (Bam earthquake, recorded at Bam station) and their response spectrum for the period interval of 0.02 to 1.0 sec. In addition, the Fourier spectrum of both as recorded and modified motion is displayed in Figure (5). It can be seen that the response spectrum of as recorded motion is higher than target spectrum for periods between 0.1 and about 0.22 sec (very short periods). For periods longer than 0.22, the aforementioned response spectrum is below the target. As shown, the MME method has successfully reduced the contribution of short period waves and strengthened the longer ones. The same can be drawn from Fourier spectra. It is clearly visible the ordinates of Fourier amplitude for modified motion are higher than as recorded motion for short frequencies, which is in complete agreement with findings from response spectra.

To further examine the performance of the method, the response spectrum of all modified motions and their corresponding mean for all three period intervals have been demonstrated in Figure (6). The errors above each plot are the mean and maximum errors of mean spectrum with respect to target. It can be readily inferred from Figure (6) that as period gets longer, the error rate decreases. That is, MME method works better for longer periods in comparison to shorter ones. Since the sensitivity of response to ground acceleration in short periods is much higher than long periods, the above observed results are not unexpected. Also, this can be viewed in terms of standard deviation. For this purpose, the standard deviation (STD) was evaluated by Equation (14):

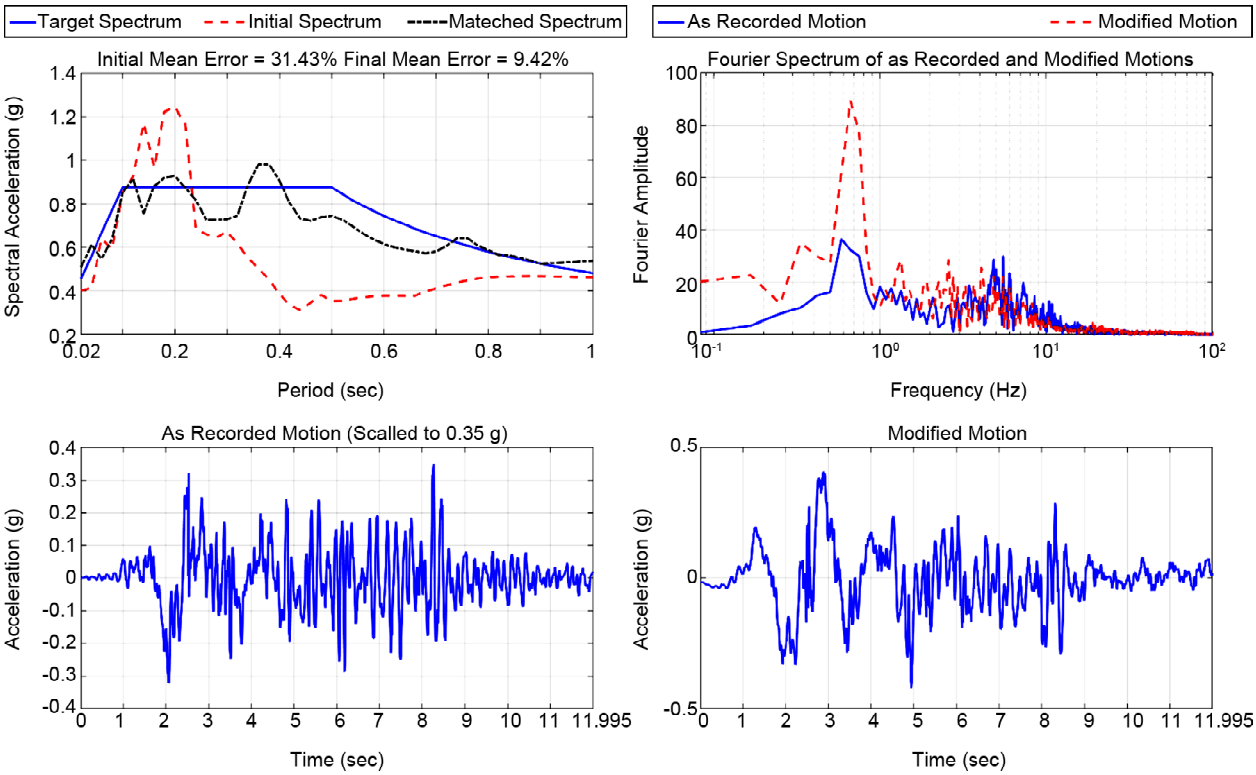

Figure 5. Spectral matching for EQ21 (MME method).

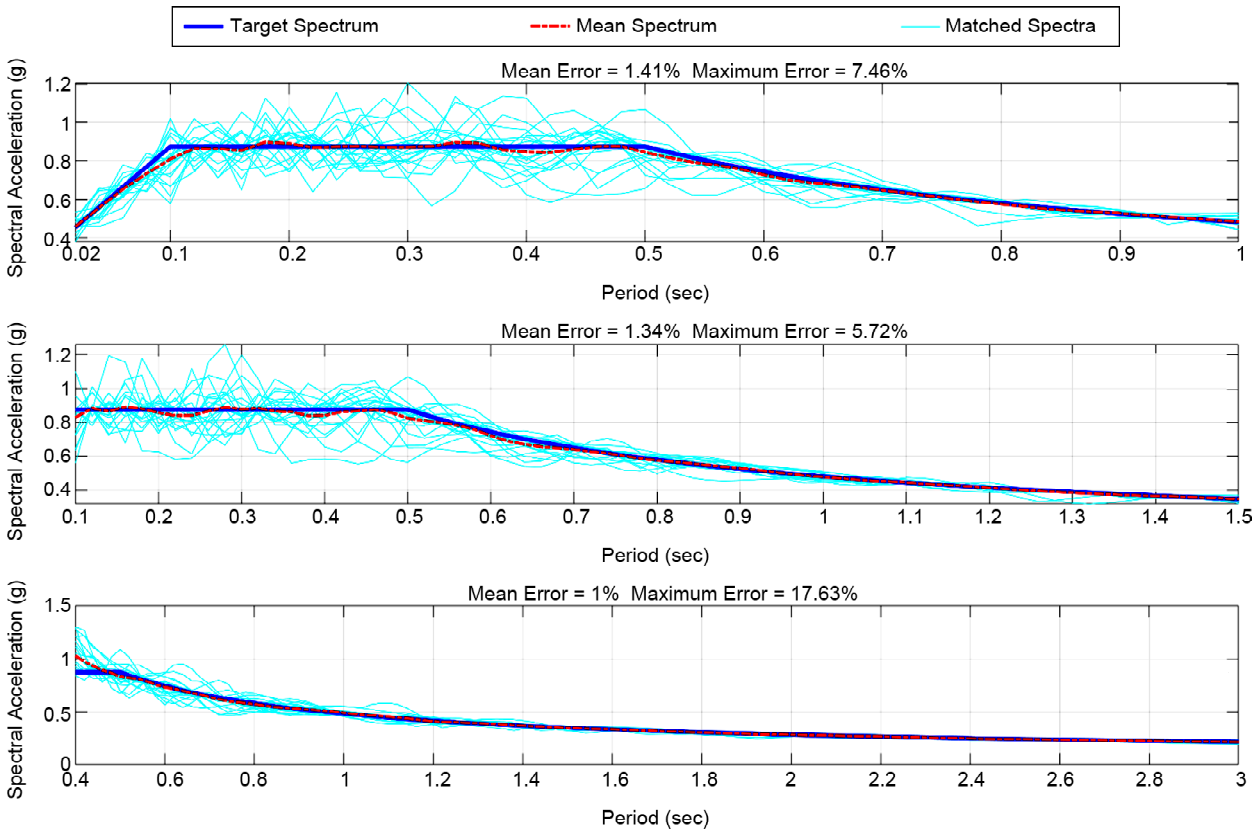

Figure 6. Matched spectra and mean of them for all period intervals (MME Method).

$$STD(T_i)=\sqrt{\frac{1}{N}\sum_{k=1}^{N}(E_k(T_i)-\mu(T_i))^2} \quad (14.1)$$

$$\mu(T_i)=\frac{1}{N}\sum_{k=1}^{N}E_k(T_i) \quad (14.2)$$

where $\mu(T_i)$ is the mean of matched spectra at period T_i, N is the number of selected records, $E_k(T_i)$ is the error of spectral acceleration at period T_i for k^{th} matched spectrum with respect to the target.

Figure (7) demonstrates the STD variation for all period intervals. As it is depicted in Figure (7), variation of the STD against period shows an approximately regular decreasing trend for periods longer than $T > 0.5$ sec. This confirms the afore-mentioned claim that MME method works better for longer periods.

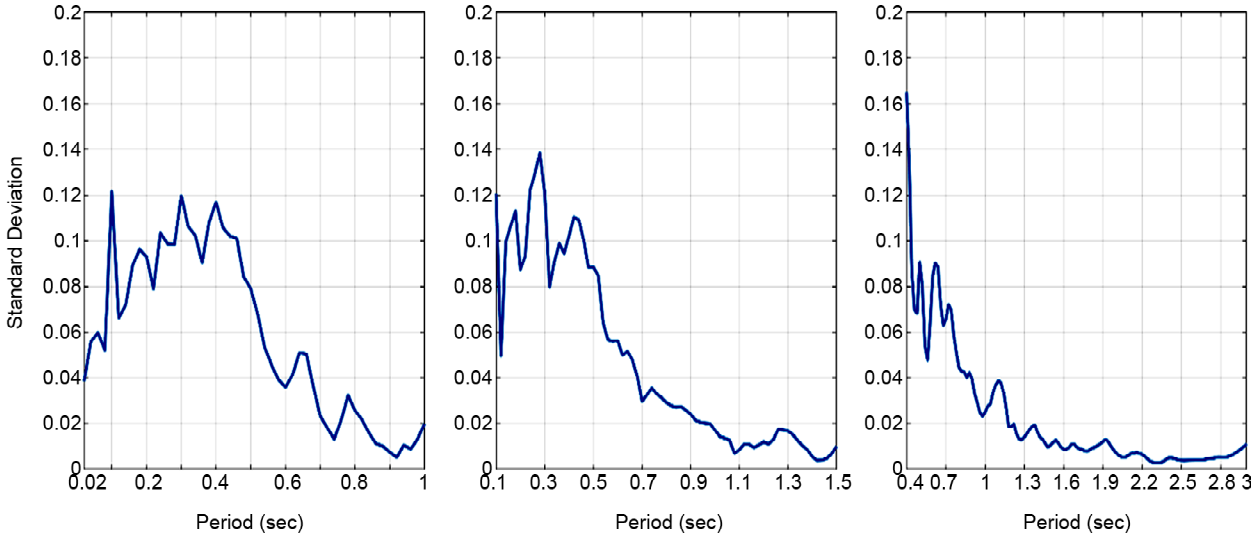

Figure 7. Variation of standard deviation against period (MME method).

4.2. Results of MEA Method

Figure (8) shows the results of application of MEA method to modify EQ01 for the period interval of 0.02 to 1.0 sec.

Response spectrum of EQ01 has initially a mean error of 35.34% with respect to the target spectrum. However after spectral matching using MEA method, the mean error was reduced to 7.65%. It is worth mentioning that for periods longer than 0.4 sec, the ordinates were amplified to match the target spectrum. The same can be seen in Fourier spectra, where low frequency components have been strengthened to generate a more compatible accelerogram.

The performance of MEA method can be examined in more detail in Figure (9), where matched spectra and their mean have been plotted. The errors above each plot are the mean and maximum errors of mean spectrum with respect to target.

Again, it can be concluded from Figure (9) that the performance of MEA method is enhanced as period elongates, and this could be attributed to lower sensitivity of response to ground acceleration for longer periods. Examination of results using the STD clearly demonstrates better performance of the method for longer periods (Figure 10). Figure (10) shows that as period increases, the STD decreases, which is in complete agreement with the conclusion derived from Figure (9).

4.3. Comparison between MME and MEA Methods

As described in previous sections, MME and MEA can be used as two efficient criteria to numerically solve Equation (7). Since these two methods employ two different criteria for optimization, final results would be different, and this can be found out by comparing the results depicted in Figures (6) and (9) in terms of mean and maximum errors. In this section, two methods would be examined by evaluating the distribution of error over spectral matching period.

Various methods for generation of spectrum compatible ground motions always possess some level of errors.

Usually, it is not possible to exactly match the response spectrum with target, thus to limit and prevent concentration of errors on a narrow band of periods, it is necessary to precisely investigate distribution of error over spectral matching period interval.

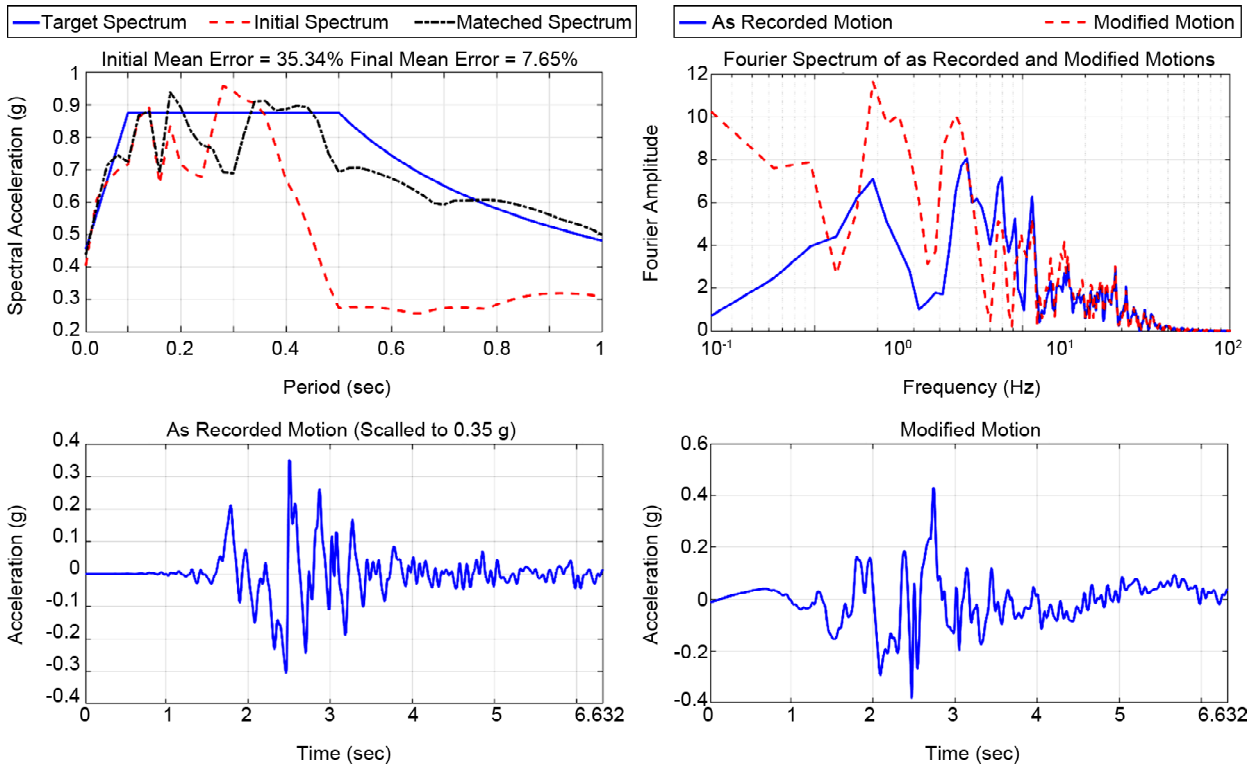

Figure 8. Spectral matching for EQ01 (MEA method).

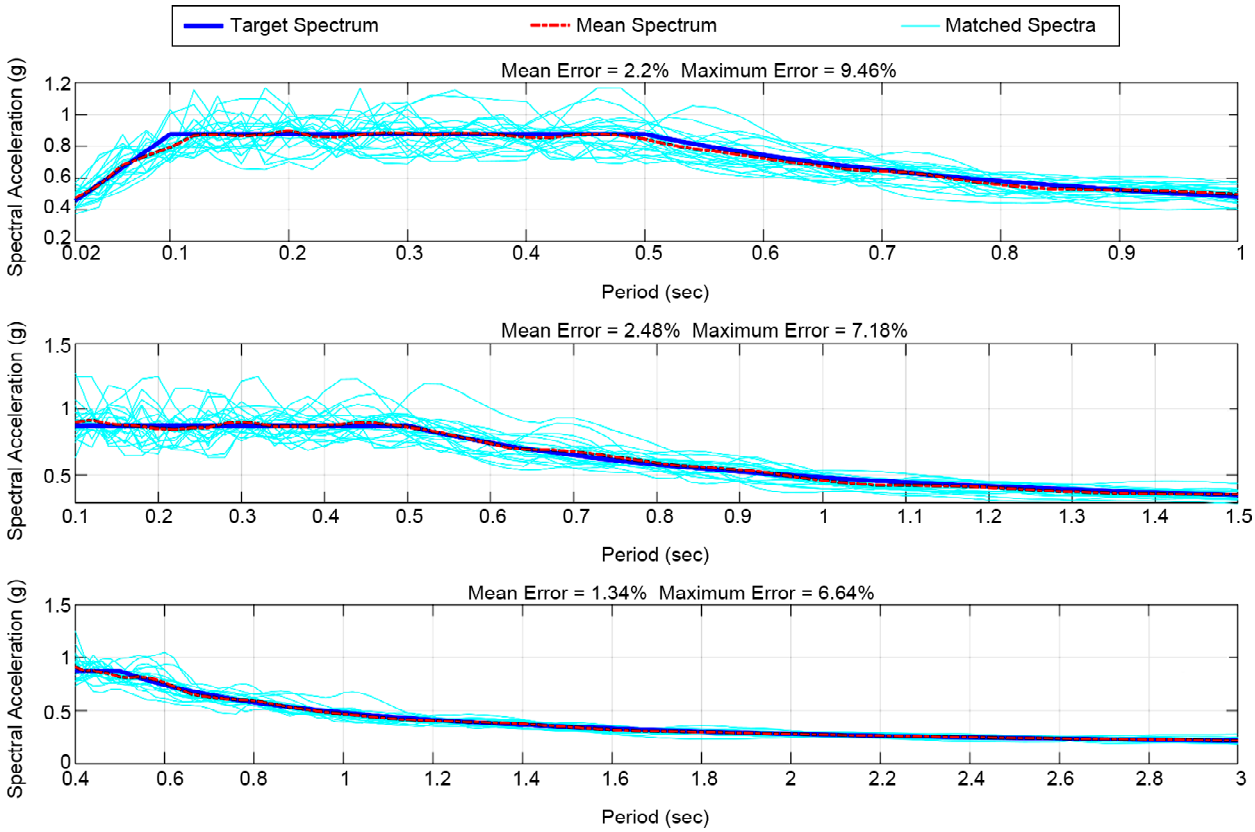

Figure 9. Matched spectra and mean of them for all period intervals (MEA Method).

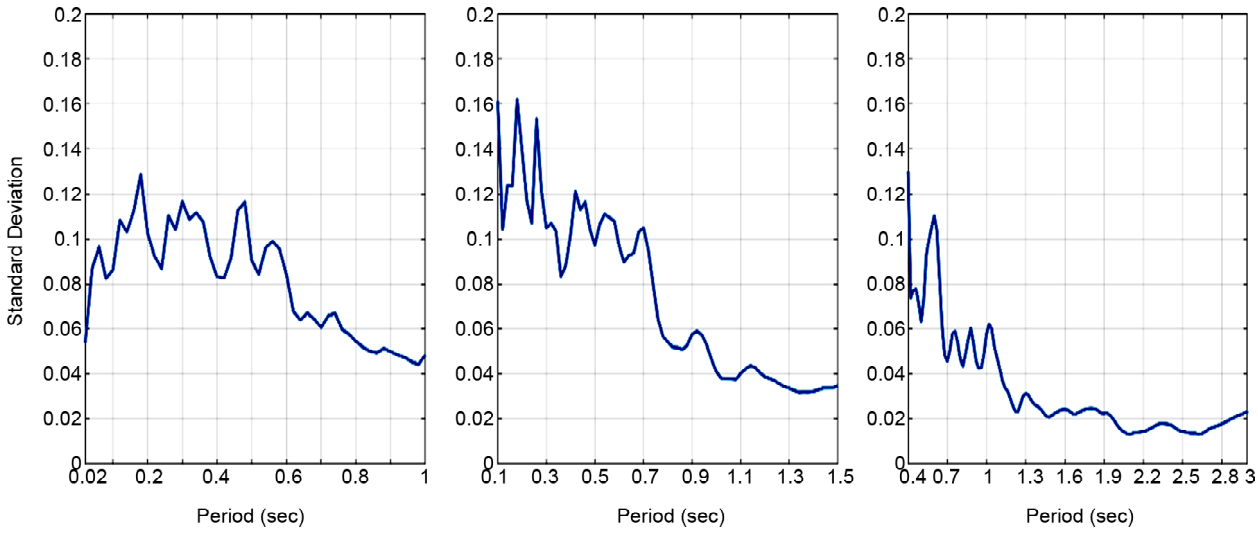

Figure 10. Variation of standard deviation against period (MEA method).

In this study, the uniformity of error distribution has been examined by comparing mean errors (E_{mean}) and the corresponding ratio of maximum to mean errors (E_{max} / E_{mean}) observed for the response spectrum of a modified accelerogram. To this end, the comparison between the values of E_{mean} and E_{max} / E_{mean} ratios has been shown in Figure (11), in which the left plots show Emean and the right ones depict the corresponding ratio of E_{max} / E_{mean} for each period interval for both criteria.

As shown in the plots on the left, in only two cases, the value of E_{mean} resulting from the MME method is slightly higher than the E_{mean} of the MEA method (EQ06 for $0.02 < T < 1.0$ sec and EQ05 for $0.4 < T < 3.0$ sec, less than 1.5% for both cases). This means that using the MME criterion will generally result in a lower E_{mean}. It should

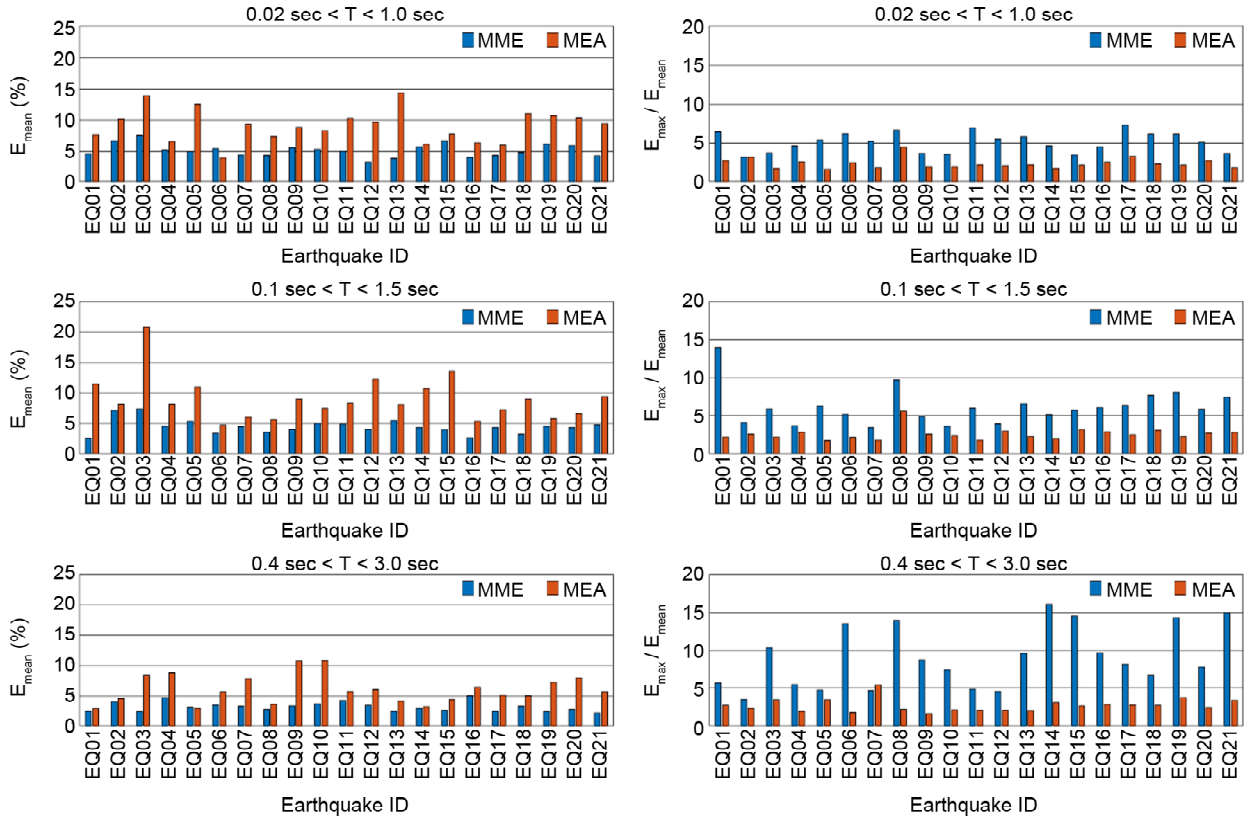

Figure 11. Comparison between mean and maximum errors for MME and MEA methods.

also be noted that for all cases, MME method is resulted in E_{mean} less than 10% while E_{mean} achieved by MEA method less than 15% (except for EQ03 on $0.1 < T < 1.5$ sec that shows E_{mean} = 21%). Therefore, it can be concluded that both methods ultimately lead to an appropriate and acceptable level of E_{mean}.

On the other hand, from the plots on the right, it can be readily inferred that in all cases the ratio of E_{max} / E_{mean} for MME method is greater than the MEA method (Except for EQ07 on $0.4 < T < 3.0$ sec). That is, although the MME criterion produces a lower E_{mean}, it should be expected that a larger E_{max} be obtained compared to the MEA criterion.

Based on the above, it can be argued that by using the MEA criterion to generate artificial accelerograms, the error distribution over the desired periodic interval will be obtained more uniformly than the MME criterion. It should be noted that the error distribution can significantly affect the dynamic response of structures. High concentration of error on a narrow band of periods may lead to overestimating or underestimating the response participation of those structural vibrational modes, which are located on that period band.

Therefore, if the mean error is more important for synthesizing seismic signals, then the MME criterion should be used. But if the priority is achieving more uniform distribution of the error, the MEA method will be more appropriate.

4.3. Comparison of Results with SeismoMatch

In this section, it is aimed to compare the results of proposed method in this work with SeismoMatch software developed by Seismosoft for generating of spectrum compatible accelerograms. This software employs wavelet transform techniques for modifying the frequency content of input seismic signals to match them with prescribed target spectrum. To this end, the three records EQ06, EQ14 and EQ16 from Table (1) were randomly selected and scaled to 0.35 g to be fed to SeismoMatch for spectral matching over the period interval of 0.02 to 1.0 sec.

Figure (12) shows the target spectrum, initial response spectra and the matched ones using SeismoMatch, MME and MEA methods for the periods range from 0.02 to 1.0 sec. As shown, the

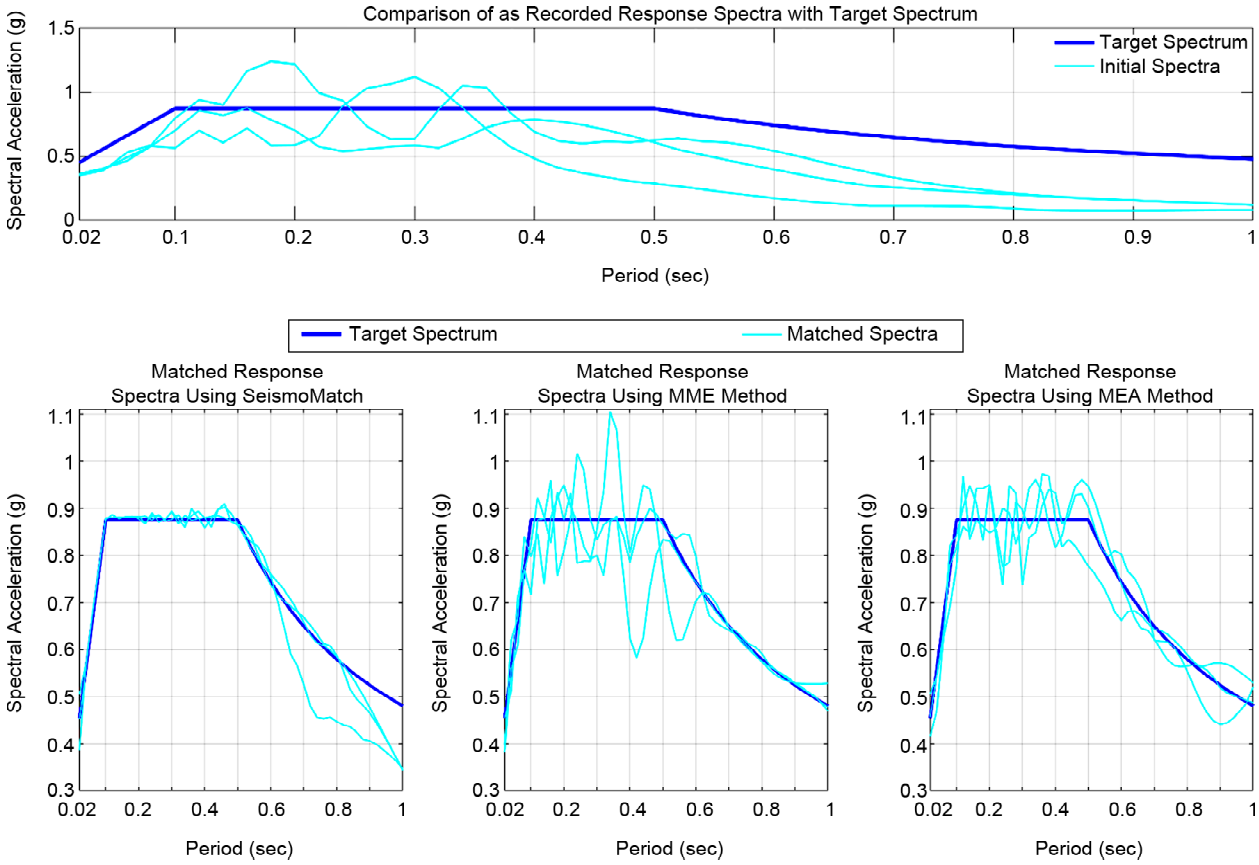

Figure 12. Spectral Matching Comparison of EQ06, EQ14 and EQ16 using SeismoMatch, MME and MEA methods.

response spectra of recorded motions are below the target for periods shorter than 0.1 sec and longer than 0.4 sec. Comparing the matched spectra, it can be readily observed that all the three methods work well for very short periods (shorter than 0.1 sec). For the periods between 0.1 and 0.6 sec, the SeismoMatch provide much closed matching results in comparison to MME and MEA methods. Where periods are longer than 0.6 sec, the MME method gives better spectral matching. As stated above, the response spectra of recorded motions are below the target for longer periods, and MME method aims this interval very well. On the other hand, applying the MME method leads to some fluctuations in the response spectrum for periods range from 0.1 to 0.4 sec.

Given the MEA method, it has lower matching level with respect to MEA method for periods longer than 0.6 sec. However, it provides smoother response spectra with errors distributed more evenly on the period interval of spectral matching and avoids the concentration of large errors (as outlined in section 4.3).

To examine in more details, the mean response spectrum of recorded and modified motions using all three methods are depicted in Figure (13) for selected records in this section. As demonstrated, the mean spectra of all three methods are in good agreement with the target in general. For periods shorter than 0.1 sec, the results are nearly the same. On the other hand, the MME and MEA methods provide more matched mean spectrum with respect to SeismoMatch for periods longer than 0.6 sec. It can be seen that as period gets longer, the difference between mean spectrum of SeismoMatch and target spectrum increases. Finally, for the period interval of 0.1 to 0.5 sec, the SeismoMatch resulted in higher level of spectral matching.

It is worth mentioning that using SeismoMatch requires a deep understanding of time-frequency analysis techniques to be able to efficiently use it. In the Help menu of this software, where it provides a brief description of the matching parameters needed to be set, it is stated that "they (matching parameters) are really intended for expert users that may be very familiar with the algorithm and the corresponding scientific publications". Such

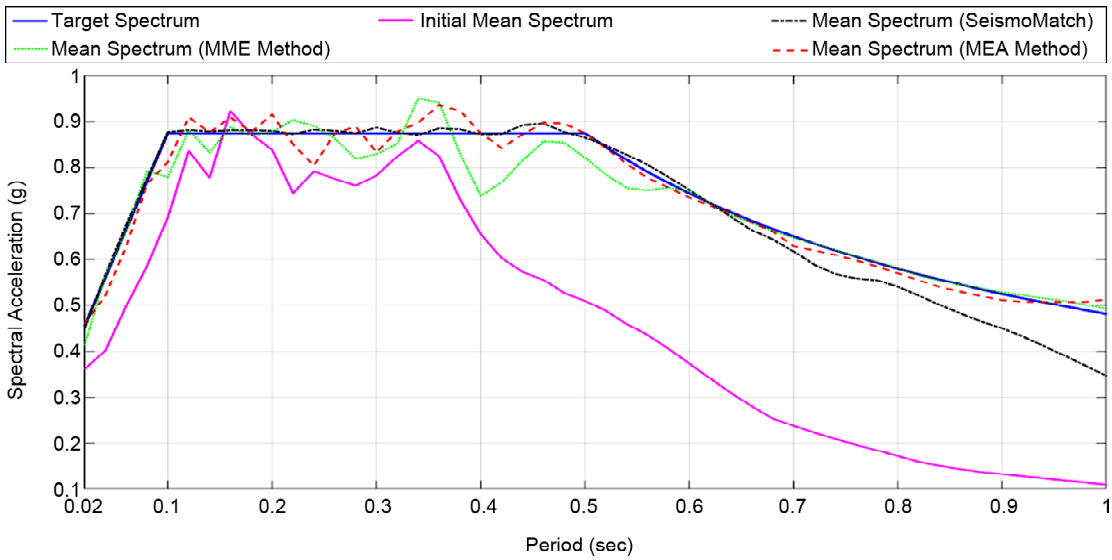

Figure 13. Comparison of the mean spectrum of as recorded and modified EQ06, EQ14 and EQ16 using SeismoMatch, MME and MEA methods.

complexities may lead to some difficulties for engineers to use the software. The proposed method may outcompete software like SeismoMatch in this area. Given the fact that the mean spectrum of modified motions using SeismoMatch, MME and MEA methods are in good agreement with the target spectrum, one can simply use the developed method in this paper confidently.

6. Dynamic Analysis Using Modified Ground Motions

6.1. Structural Models

Two 2-dimensional steel moment resisting frames of 3 and 12 stories have been designed according to Iran's code for design and construction of steel structures (tenth Regulation of National Building Code, 2022) and Iran Seismic Code (Standard 2800). Figure (14) displays the elevation view of structural models. Main structural properties of steel frames are given in Table (3). Given the fundamental mode period of models, the 0.2 and 1.5 times of this period were selected as T_i and T_f for spectral matching period interval. Note that Ti and Tf have been rounded down and up respectively to the nearest tenth.

Table 3. Structural properties of 2-dimensional models.

No. of Stories	Story Height (m)	No. of Bays	Bay Width (m)	First Mode Period (sec)	T_i (sec)	T_f (sec)
3	3.2	4	4	0.81	0.16	1.30
12	3.2	4	4	2.05	0.40	3.10

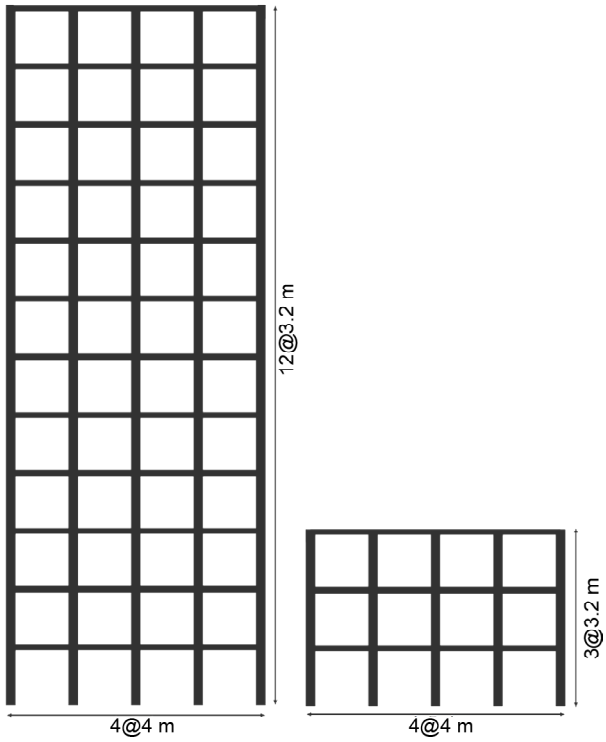

Figure 14. Elevation view of 2-dimensional steel moment resisting frames.

6.2. Selected Records for Dynamic Analysis

Seven earthquake records were selected randomly from Table (1) to be used in this section. These records are: EQ04, EQ05, EQ08, EQ09, EQ17, EQ18 and EQ21. The selected records have been modified using MME, MEA methods as well as SeismoMatch. It is worth mentioning that these records were scaled to 0.35 g before triggering the spectral matching process.

In addition, selected records for dynamic analysis of structures were scaled using the procedure provided by Standard 2800. To this end, the records were initially scaled to 1.0 g and then the mean of their acceleration response spectra have been calculated and compared with the standard design spectrum (evaluated using the procedure described in section 2.1). The scale factor was selected such that the mean spectrum not to be less than the standard design spectrum in any period. Figure (15) depicts the mean spectra evaluated using the four afore-mentioned methods and compares it with standard design spectrum on specified period intervals for spectral matching in Table (3).

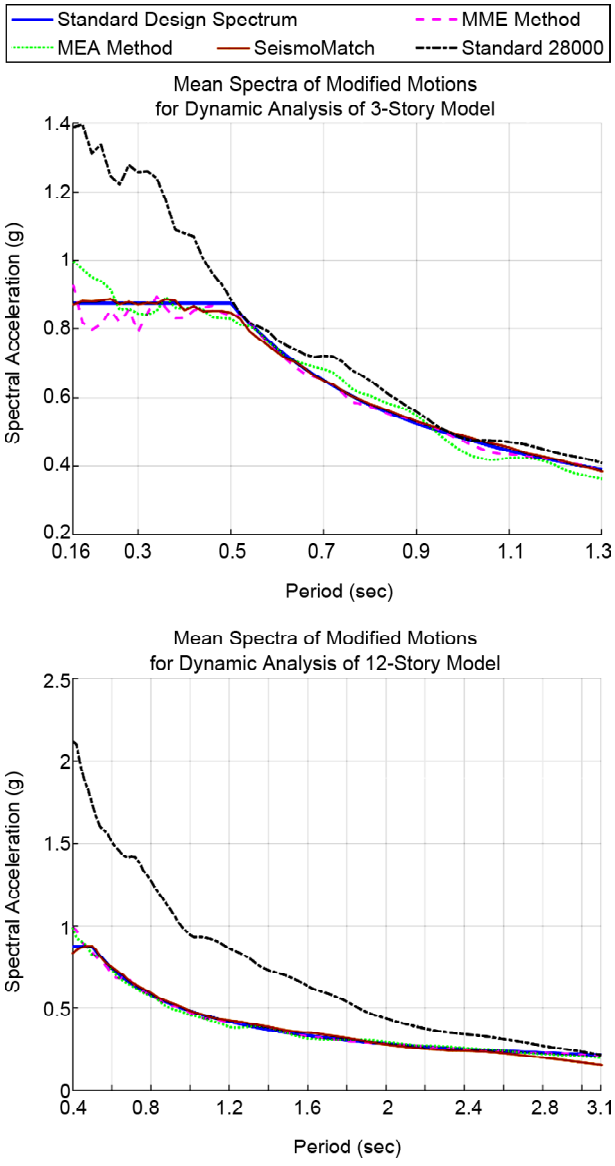

Figure 15. Comparison of mean spectra of modified motions with standard design spectrum for dynamic analysis of 2-dimensional models.

As shown in Figure (15), for mean spectra of MME and MEA methods as well as SeismoMatch, there is a close agreement with standard design spectrum. The mean spectra resulted from SeismoMatch in 0.40 to 3.10 sec spectral matching period interval, starts to deviate from the target for periods longer than 2.6. This result was expected as outlined in section 5.

The mean spectrum evaluated using the procedure of Standard 2800, is above the target for periods shorter than 0.5 sec for the spectral matching period interval of 0.16 to 1.3 sec. The situation worsens for the period range of 0.40 to 3.10 sec, where the mean spectrum resulted from Standard 2800 is above the target all over the period interval. One may expect some bias in dynamic response of structures under scaled records using the Standard 2800.

6.3. Comparison of Dynamic Responses

The modified ground motions were applied to 2-dimensional models and linear dynamic analysis have been conducted using constant average acceleration method (also known as Newmark - $\beta = 1/4$ method). The maximum drift of roof floor with respect to ground have been extracted and employed as a global response of structures to assess their performance.

The maximum roof drift and corresponding average and standard deviation are demonstrated in Figure (16) for 3-story model. It is clearly visible that the scaled records using the Standard 2800 have led to higher scatter in maximum roof drift response. On the other hand, the maximum roof drift responses evaluated from modified records using MEA and MME methods as well as SeismoMatch are close together. One can readily conclude that the spectral matching using MME and MEA methods can result in dynamic response distribution close to modified earthquake records using SeismoMatch. This proves the capability of proposed method for ground motion simulation. The comparison of standard deviations calculated for maximum roof drift clearly shows the scattering of responses when records are scaled using Standard 2800 with respect to others.

The same applies to 12-story model and the results are being shown in Figure (17). In this case

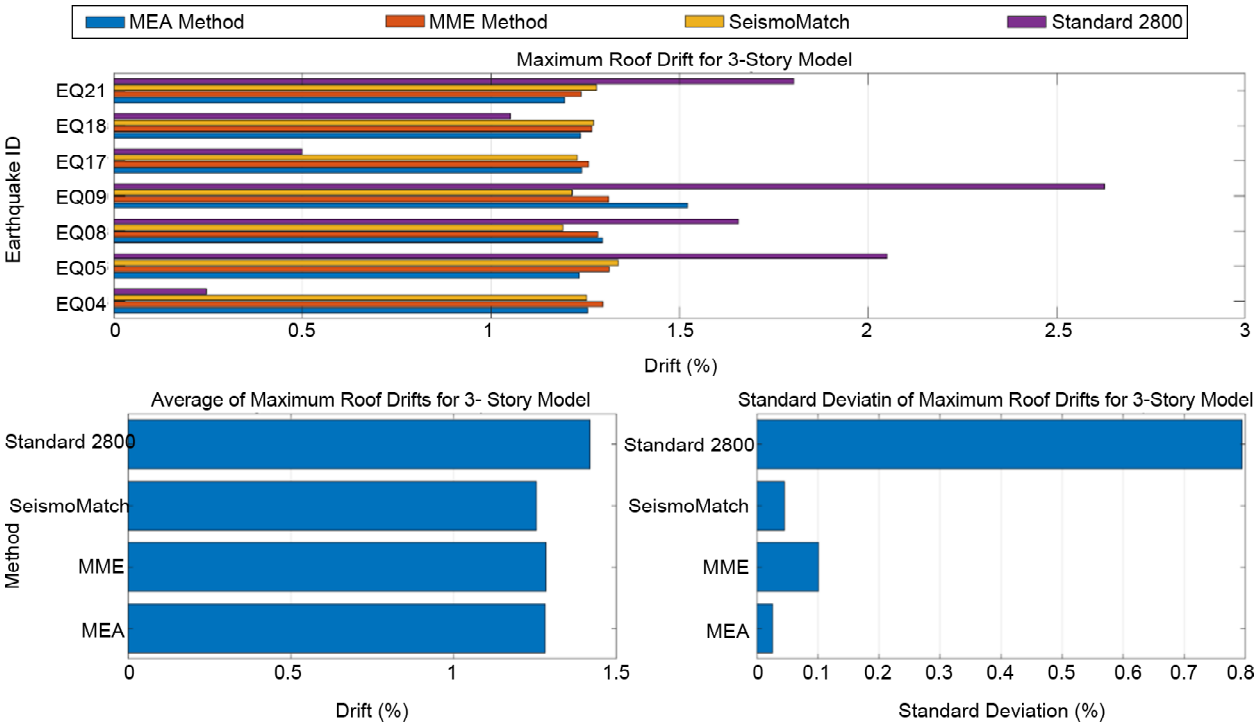

Figure 16. Comparison of Maximum roof drifts for 3-story model.

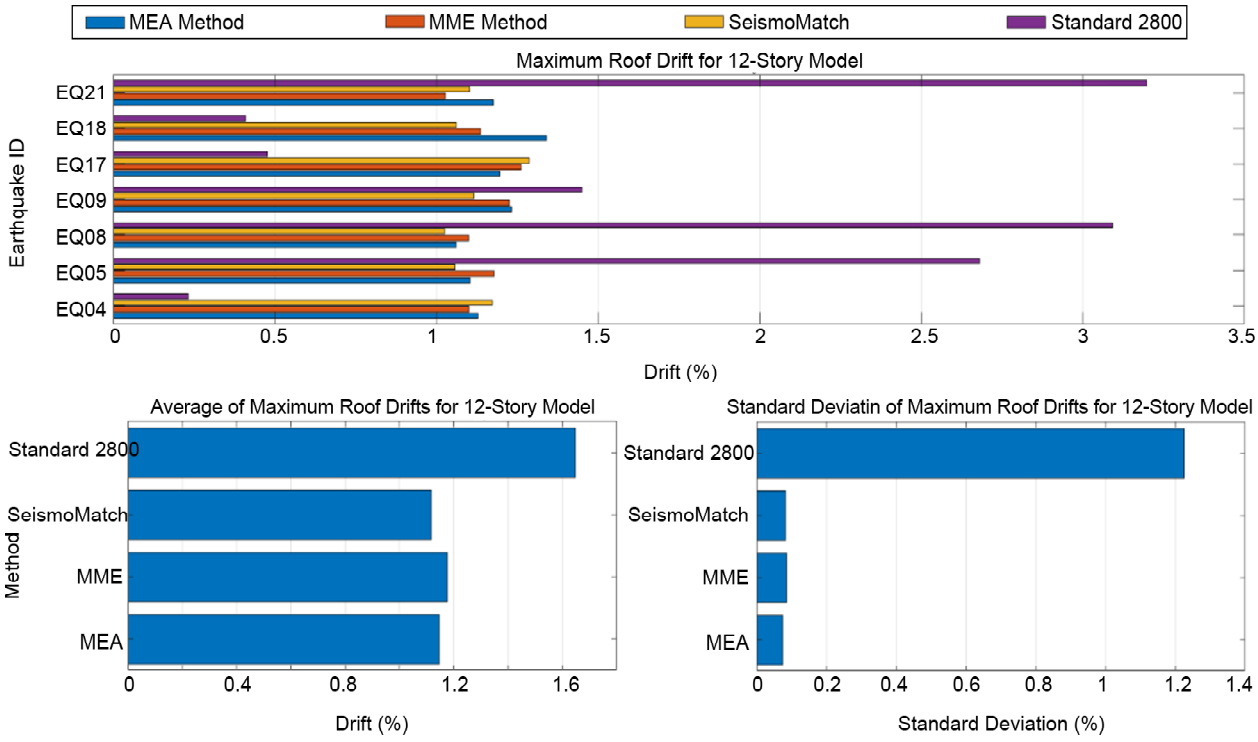

Figure 17. Comparison of Maximum roof drifts for 12-story model.

also, the bias introduced to maximum roof drift from records scaled by the method of Standard 2800 can be observed clearly with respect to modified motions using MME and MEA methods and SeismoMatch. This is in consistence with mean spectra demonstrated in Figure (15).

7. Conclusions

A simple but practical numerical iterative procedure for generation of spectrum compatible accelerograms was proposed. Just basic concepts of structural dynamics are required to be able to effectively use the proposed method, and this

makes this procedure be welcomed by the engineering community.

The following results can be deduced from the study:

- Two criteria (MME and MEA methods) have been applied to modify seed records such that their response spectrum get as close as possible to target spectrum.
- Both criteria for generation of spectrum compatible accelerograms works better as period gets longer. Careful examination of standard deviations proves this claim.
- Generally, application of MEA method results in higher mean error but lower maximum error in comparison to MME method. That is, MEA method provides better error distribution over spectral matching period interval.
- If lower mean error is desired, MME criterion must be employed for generation of artificial accelerograms.
- If more uniform error distribution over spectral matching period is of higher importance, applying MEA criterion is preferable.
- To prevent overestimation or underestimation of contribution of some vibrational modes, MEA method can be employed.
- The comparison of results with benchmark method employed by SeismoMatch software proves the capability of the proposed method for ground motion simulation.

References

Amiri, G.G., Abdolahi Rad, A., Aghajari, S., & Khanmohamadi Hazaveh, N. (2012). Generation of near-field artificial ground motions compatible with median-predicted spectra using PSO-based neural network and wavelet analysis. *Computing in Civil and Infrastructure Engineering*, *27*(9), 711-730. doi:10.1111/j.1467-8667.2012.00783.x.

Amiri, G.G., Bagheri, A., & Seyed Razaghi, S. A. (2009). Generation of multiple earthquake accelerograms compatible with spectrum via the wavelet packet transform and stochastic neural networks. *Journal of Earthquake Engineering*, *13*(7), 899-915. doi:10.1080/13632460802687728.

Amiri, G.G., Rad, A.A., & Hazaveh, N.K. (2014). Wavelet-based method for generating nonstationary artificial pulse-like near-fault ground motions. *Computing in Civil and Infrastructure Engineering*, *29*(10), 758-770. doi:10.1111/mice.12110.

Bani-Hani, K.A., & Malkawi, A.I. (2017). A Multi-step approach to generate response-spectrum-compatible artificial earthquake accelerograms. *Soil Dynamics and Earthquake Engineering*, *97*, 117-132. doi:10.1016/j.soildyn.2017.03.012.

Batou, A., & Soize, C. (2014). Generation of accelerograms compatible with design specifications using information theory. *Bulletin of Earthquake Engineering*, *12*(2), 769-794. doi:10.1007/s10518-013-9547-z.

Bazrafshan, A., & Khaji, N. (2020). Generation of synthetic accelerograms using a probabilistic critical excitation method based on energy constraint. *Earthquakes and Structures*, *18*(1), 45-56. doi:10.12989/eas.2020.18.1.045.

Brewick, P.T., Hernandez-Garcia, M., Masri, S.F., & Smyth, A.W. (2018). A data-based probabilistic approach for the generation of spectra-compatible time-history records. *Journal of Earthquake Engineering*, *22*(8), 1365-1391. doi:10.1080/13632469.2017.1286618.

Cacciola, P., & Zentner, I. (2012). Generation of response-spectrum-compatible artificial earthquake accelerograms with random joint time-frequency distributions. *Probabilistic Engineering Mechanics*, *28*, 52-58. doi:10.1016/j.probengmech.2011.08.004.

Carli, F., & Carino, C. (2016). Evolutionary model for synthetic spectrum-compatible accelerograms. In: *Springer Proceedings in Mathematics and Statistics*, *181*, 131-141. doi:10.1007/978-3-319-42402-6_12.

Cecini, D., & Palmeri, A. (2015). Spectrum-compatible accelerograms with harmonic wavelets. *Computers & Structures*, *147*, 26-35. doi:10.1016/j.compstruc.2014.10.013.

Das, S., & Gupta, V. K. (2008). Wavelet-based simulation of spectrum-compatible aftershock accelerograms. *Earthquake Engineering & Structural Dynamics*, *37*(11), 1333-1348. doi:10.1002/eqe.820.

Fan, J., Yong, Y., & Zhang, Y. (2010). Time-frequency analysis and artificial adjustment of earthquake gound motions via S-transform. *Earth and Space*, 3101-3110. doi:10.1061/41096(366)295.

Gascot, R.L., & Montejo, L.A. (2016). Spectrum-compatible earthquake records and their influence on the seismic response of reinforced concrete structures. *Earthquake Spectra*, *32*(1), 101-123. doi:10.1193/011714EQS010M.

Gholizad, A., & Pursadrollah, A. (2017). Quantitative evaluation of near-fault records generated via wavelet transform. *Journal of Structural Engineering and Earthquake Engineering*, *19*(1), 1-11.

Giaralis, A., & Spanos, P.D. (2009). Wavelet-based response spectrum compatible synthesis of accelerograms-Eurocode application (EC8). *Soil Dynamics and Earthquake Engineering*, *29*(1), 219-235. doi:10.1016/j.soildyn.2007.12.002.

Giaralis, A., & Spanos, P.D. (2012). Derivation of response spectrum compatible non-stationary stochastic processes relying on Monte Carlo-based peak factor estimation. *Earthquakes and Structures*, *3*(3), 581-609. doi:https://doi.org/10.12989/eas.2012.3.3.581.

Gomes, R.C., Santos, J., & Oliveir, C.S. (2006). Design spectrum-compatible time histories for numerical analysis: Generation, correction, and selection. *Journal of Earthquake Engineering*, *10*(6), 843-865. doi:10.1080/13632460609350620.

Huang, D., & Wang, G. (2017). Energy-Compatible and Spectrum-Compatible (ECSC) ground motion simulation using wavelet packets. *Earthquake Engineering & Structural Dynamics*, *46*(11), 1855-1873. doi:10.1002/eqe.2887.

Li, Z., Kotronis, P., & Wu, H. (2017). Simplified approaches for Arias Intensity correction of synthetic accelerograms. *Bulletin of Earthquake Engineering*, *15*(10), 4067-4087. doi:10.1007/s10518-017-0126-6.

Liu, Z., Du, C., Yuan, J., & Jiang, S. (2009). Numerical simulation of nonstationary earthquake field compatible with prescribed response spectrum. *TCLEE* 2009, *357*, 1-11. doi:10.1061/41050(357)102.

Mitropoulou, C.C., Lagaros, N.D., & Papadrakakis, M. (2015). Generation of artificial accelerograms for efficient life-cycle cost analysis of structures. *Engineering Structures*, *88*, 138-153. doi:10.1016/j.engstruct.2015.01.029.

Mukhopadhyay, S., Das, S., & Gupta, V.K. (2019). Wavelet-based generation of accelerogram-consistent, spectrum-compatible motions: New algorithms and short-period overestimation. *Soil Dynamics and Earthquake Engineering*, *121*, 327-340. doi:10.1016/j.soildyn.2019.02.001.

Parajuli, H.R., & Shrestha, R.K. (2018). Generation of synthetic ground motion. *Journal of Geological Resources Engineering*, 6, 105-111. doi:https://doi.org/10.17265/2328-2193/2018.03.002.

Rajabi, E., & Ghodrati Amiri, G. (2020). Generation of critical aftershocks using stochastic neural networks and wavelet packet transform. *Journal of Vibration Control*, *26*(5-6), 331-351. doi:10.1177/1077546319879536.

Rajasekaran, S., Latha, V., & Lee, S.C. (2006). Generation of artificial earthquake motion records using wavelets and principal component analysis. *Journal of Earthquake Engineering*, *10*(5), 665-669. doi:10.1080/13632460609350614.

Road, Housing & Urban Development Research Center (2017). *Iranian Code of Practice for Seismic Resistant Design of Buildings*, 4th Edition,

Rofooei, F.R., Mobarake, A., & Ahmadi, G. (2001). Generation of artificial earthquake records with a nonstationary Kanai-Tajimi model. *Engineering Structures*, *23*(7), 827-837. doi:10.1016/S0141-0296(00)00093-6.

Sarkar, K., Gupta, V.K., & George, R.C. (2016). Wavelet-based generation of spatially correlated accelerograms. *Soil Dynamics and Earthquake Engineering*, 87, 116-124. doi:10.1016/j.soildyn.2016.05.005.

Shama, A. (2012). Spectrum compatible earthquake ground motions by morlet wavelet. In: *20th Analysis and Computation Specialty Conference*, 163-172. doi:10.1061/9780784412374.015.

Shields, M. D. (2015). Simulation of spatially correlated nonstationary response spectrum-

compatible ground motion time histories. *Journal of Engineering Mechanics*, *141*(6), 04014161. doi:10.1061/(ASCE)EM.1943-7889.0000884.

Spanos, P.D., Giaralis, A., & Jie, L. (2009). Synthesis of accelerograms compatible with the Chinese GB 50011-2001 design spectrum via harmonic wavelets: Artificial and historic records. *Earthquake Engineering and Engineering Vibration*, *8*(2), 189-206. doi:10.1007/s11803-009-9017-4.

Suarez, L.E., & Montejo, L.A. (2005). Generation of artificial earthquakes via the wavelet transform. *International Journal of Solids and Structures*, *42*, 5905-5919. doi:10.1016/j.ijsolstr.2005.03.025.

Tehrani, M.H., & Harvey, P.S. (2019). Generation of synthetic accelerograms for telecommunications equipment: fragility assessment of a rolling isolation system. *Bulletin of Earthquake Engineering*, *17*(3), 1715-1737. doi:10.1007/s10518-018-0505-7.

Tenth Regulation of National Building Code-Design and Construction of Steel Structures (2022). *5th Edition. Office of National Regulations and Building Control of the Ministry of Roads and Urban Development.*

Trovato, S., D'Amore, E., Yue, Q., & Spanos, P.D. (2017). An approach for synthesizing tri-component ground motions compatible with hazard-consistent target spectrum - Italian aseismic code application. *Soil Dynamics and Earthquake Engineering*, *93*, 121-134. doi:10.1016/j.soildyn.2016.12.003.

Tsioulou, A., Taflanidis, A.A., & Galasso, C. (2018). Modification of stochastic ground motion models for matching target intensity measures. *Earthquake Engineering & Structural Dynamics*, *47*(1), 3-24. doi:10.1002/eqe.2933.

Vetter, C.R., Taflanidis, A.A., & Mavroeidis, G.P. (2016). Tuning of stochastic ground motion models for compatibility with ground motion prediction equations. *Earthquake Engineering & Structural Dynamics*, *45*(6), 893-912. doi:10.1002/eqe.2690.

Vrochidou, E., Alvanitopoulos, P., Andreadis, I., & Elenas, A. (2018). Artificial accelerograms composition based on the CEEMD. *Transactions of the Institute of Measurement and Control*, *40*(1), 239-250. doi:10.1177/0142331216654533.

Vrochidou, E., Alvanitopoulos, P., Andreadis, I., Elenas, A., & Mallousi, K. (2014). HHT-based artificial seismic accelerograms generation. *IFIP Advances in Information and Communication Technology*, *436*, 476-486. doi:10.1007/978-3-662-44654-6_47.

Wang, S., Yu, R., De Risi, R., & Li, X. (2021). A new energy-compatible nonstationary stochastic ground-motion simulation method. *Earthquake Engineering & Structural Dynamics*. doi:10.1002/eqe.3428.

Wang, S., Yu, R., Li, X., & Lv, H. (2019). Simulation method of ground motion matching for multiple targets and effects of fitting parameter variation on the distribution of PGD. *Earthquakes and Structures*, *16*(5), 563-573. doi:https://doi.org/10.12989/eas.2019.16.5.563.

Zhang, C.R., Chen, H.Q., & Li, M. (2007). Earthquake accelerogram simulation with statistical law of evolutionary power spectrum. *Acta Seismologica Sinica (English Edition)*, *20*(4), 435-446. doi:10.1007/s11589-007-0435-y.

Nomenclature

A: base design acceleration
$A(t)$: modified ground acceleration
B: represents spectrum shape factor
E: error
E_m: mean error
EMD: empirical mode decomposition
IMF: intrinsic mode function
$L(t)$: lower envelope
$m(t)$: mean envelope
MEA: minimum enclosed area
MME: minimum mean error
N: spectrum correction factor
PGA: peak ground acceleration
R: closest distance to fault
$r(t)$: residual
R_{ij}: acceleration response time history
Sa: response spectrum
Sa_L: lower envelope spectrum
Sa_t: target spectrum
Sa_U: upper envelope spectrum
S_b: base signal

STD: standard deviation
T: period
T_f: final period
T_i: initial period
$U(t)$: upper envelope
V_{s30}: average shear wave velocity of top 30 m of the site
α: scale factor for base signals
β: ratio of target spectrum to response spectrum
θ: final scale factor in MEA method
μ: mean of matched spectra